JOURNAL OF GEOPHYSICAL RESEARCH, VOL. 114, C10020, doi:10.1029/2009JC005317, 2009

A thin layer of phytoplankton observed in the Philippine Sea with a synthetic moored array of autonomous gliders

Benjamin A. Hodges[1] and David M. Fratantoni[1]

Received 6 February 2009; revised 10 June 2009; accepted 3 August 2009; published 23 October 2009.

[1] A synthetic moored array composed of five buoyancy-propelled autonomous underwater gliders was used to characterize mesoscale variability and phytoplankton distribution in a 100 km × 100 km domain in the Philippine Sea east of Luzon Strait for 10 days in May 2004. The study area, located east of the Kuroshio near the subtropical front, is dominated by strong internal tides, by energetic westward-propagating mesoscale eddies with azimuthal velocities exceeding 50 cm/s, and by a deep (130 m) maximum in chlorophyll fluorescence. Each glider in the array was instructed to maintain geographic position while repeatedly profiling to 200-m depth. Good station-keeping performance enabled the resulting series of vertical profiles to be interpreted in the same manner as a physically moored chain of instruments. Although organized primarily as a demonstration of glider capabilities, this field exercise provides a unique data set for examining biological-physical interactions in the open ocean. Here we report on the evolution of a thin layer of phytoplankton observed near the deep chlorophyll maximum. Coincident observations of fine structure in temperature and salinity suggest that the thinning process of this layer was driven primarily by physical forcing, most probably vertical shear associated with energetic diurnal internal waves, as opposed to a biological mechanism, such as convergent swimming, grazing, or spatial variation in growth rate.

Citation: Hodges, B. A., and D. M. Fratantoni (2009), A thin layer of phytoplankton observed in the Philippine Sea with a synthetic moored array of autonomous gliders, *J. Geophys. Res.*, *114*, C10020, doi:10.1029/2009JC005317.

1. Introduction

[2] Thin phytoplankton layers were first reported by *Strickland* [1968]. Since then, persistent layers with substantial horizontal extent have been observed in a variety of ocean environments [e.g., *Derenbach et al.*, 1979; *Donaghay et al.*, 1992; *Cowles and Desiderio*, 1993; *Cowles et al.*, 1998]. These layers, generally less than a few meters in vertical extent but often extending for kilometers horizontally [*Dekshenieks et al.*, 2001; *McManus et al.*, 2003], have been shown to substantially impact ecosystem dynamics and have significant optical and acoustical consequences [e.g., *Donaghay et al.*, 1992; *Zaneveld and Pegau*, 1998].

[3] Theory [e.g., *Osborn*, 1988; *Birch et al.*, 2008], numerical simulations [e.g., *Franks*, 1995], and in situ studies [e.g., *Cowles et al.*, 1998; *Cowles*, 2003] indicate that a combination of vertical stratification and the differential lateral movement of water (i.e., vertical shear) are central to the generation and persistence of vertical fine structure in both physical and biological parameters. Investigation of such phenomena requires simultaneous measurement of physical and biological ocean properties at high vertical resolution, and preferably with fine horizontal resolution and for extended periods of time. In coastal waters, recent progress has been made using specialized profiling instrumentation deployed from ships and moorings [e.g., *Dekshenieks et al.*, 2001; *Cowles*, 2003; *McManus et al.*, 2003]. However, there are few reported observations of thin layers in the open ocean, in part because coastal areas, being more accessible, have been sampled more thoroughly. We report here on the characteristics and evolution of a thin phytoplankton layer many hundreds of kilometers from shore in the western tropical Pacific, observed using a novel approach to mid-ocean data collection.

2. Methods

2.1. Platforms and Sensors

[4] Gliders [e.g., *Davis et al.*, 2002; *Rudnick et al.*, 2004] are slow-moving underwater vehicles propelled by changes in their buoyancy. The mobility, high endurance, and relatively slow ascent/descent rate of gliders make them appropriate platforms from which to observe, for example, oceanic features with broad spatial extent but small vertical scale.

[5] The vehicles used in this experiment were constructed by Webb Research Corporation of East Falmouth, Massachusetts. Each has a mass of approximately 50 kg, an overall length of approximately 1.8 m, and is powered by 220 C-size alkaline batteries contained within an aluminum pressure hull. A piston driven by an electric motor is used to

[1]Autonomous Systems Laboratory, Department of Physical Oceanography, Woods Hole Oceanographic Institution, Woods Hole, Massachusetts, USA.

0148-0227/09/2009JC005317$09.00

adjust the glider's displacement (and hence its buoyancy) through a range of about 460 cm^3. Under normal operation, the vehicle travels between the surface and a maximum depth of 200 m in a sawtooth-shaped gliding trajectory with a vertical speed near 20 cm/s, a forward speed of 45 cm/s, and effective survey speed (including time spent drifting at the surface) of about 30 cm/s. At predetermined intervals, typically spanning several hours and multiple ascent-descent cycles, the vehicle surfaces to determine its geographic position via GPS, transmit a subset of collected data via Iridium satellite telephone, and receive new navigational instructions.

[6] During the experiment described here, each glider's science payload consisted of an unpumped Sea-Bird SBE-41 CTD, a WET Labs ECO-bb2f chlorophyll fluorometer and two-channel backscatter sensor, and a custom WHOI photosynthetically active radiation (PAR) module to measure downwelling irradiance. Outputs from these sensors are recorded in the glider's internal memory at a rate of approximately 0.5 Hz, or one sample every two seconds. In addition to gathering data from these sensors, at each surfacing a glider intrinsically measures the time- and space-averaged horizontal slab velocity of the water as a by-product of navigational calculations. Glider speed through the water is estimated from the vehicle attitude (pitch and roll) and the rate of change of the measured pressure; the glider dead-reckons underwater by integrating this speed combined with its compass heading. Between one surfacing and the next, a comparison of the dead-reckoned displacement with the GPS-measured distance traveled over ground yields an estimate of the current velocity averaged temporally over the interval between surfacings and vertically over the depth of the dives. In shallow water this measurement is usually sufficient to describe the general characteristics of the background circulation. In deeper water it enables computation of absolute (i.e., unambiguous with respect to a reference layer) geostrophic velocity profiles.

[7] Gliders move slowly, but are capable of operating continuously for weeks or months. The remarkable operational endurance of gliders as compared to many other autonomous underwater vehicles (AUVs) is the result of a fundamental tradeoff between endurance and speed. The Reynolds number of an AUV may be defined as UL/ν, where U is the speed of the vehicle through the water, L is a characteristic length scale, and ν is the kinematic viscosity of the water. The Reynolds number of a glider is approximately 10^6; that of a faster AUV might be 10^7. In this Reynolds number regime, the drag coefficient of streamlined bodies typically varies relatively slowly with the Reynolds number [e.g., *Hoerner*, 1965]. The propulsive requirements therefore bear a simple relationship to a vehicle's velocity through the water: the hydrodynamic drag force is approximately proportional to its square, and the power required to overcome this drag is approximately proportional to its cube. A slow glider with a nominal speed of 0.5 m/s therefore requires less than 1% of the propulsion power needed to move at 2.5 m/s. For a given onboard energy storage capacity and hotel load (i.e., that power utilized for sensors, data telemetry, etc.), reduced speed translates directly to greater range and endurance.

[8] As a consequence of their slow forward speed, gliders often have limited maneuverability and are subject to being swept away by even moderate oceanic flows. In addition, it is often difficult to synoptically observe even a small ocean region using a single glider, as the timescale over which the intended survey volume evolves may be shorter than that required for the glider to occupy it. The latter problem is analogous to shipboard occupation of an ocean-spanning transect in which a month of distributed measurements are interpreted as a synoptic section. Unlike a glider, however, the ship's higher effective survey speed (typically 4–5 m/s) does enable substantially synoptic measurement of, for example, the mesoscale eddy field (i.e., a baroclinic deformation radius can be occupied within a fraction of an inertial period) whereas a glider's measurement of the same phenomena may be badly aliased.

2.2. Sampling Strategy

[9] An effective observational strategy that addresses the intrinsic slowness of glider navigation typically requires simultaneous operation of many vehicles [e.g., *Bellingham and Willcox*, 1996; *Fratantoni and Davis*, 2003]. Such a strategy is often necessary to avoid aliasing when gliders are used to obtain spatially distributed measurements (i.e., property mapping) along predetermined or adaptively modified tracklines [e.g., *Fiorelli et al.*, 2004].

[10] Alternatively, gliders can use their limited maneuverability to maintain geographic position and collect time series measurements at a point. This strategy can decrease the relevance of the glider's speed limitation at the obvious expense of spatial coverage. This latter mission type, which we refer to as a synthetic mooring, was utilized for the Philippine Sea work described herein.

[11] Under normal usage, the endurance of a glider is a few weeks or months, whereas traditional moorings last a year or two. The advantage of synthetic moorings over traditional ones is that they can be deployed quickly and cheaply. Several gliders can be launched at once from a research vessel, leaving the vessel free to complete other tasks or return to port while the gliders position themselves at the nodes of a predetermined array. Though promising, this mode of operation has not been used widely yet. To our knowledge, the five-node synthetic moored array discussed here is the largest yet deployed (larger fleets of gliders following other sampling schemes have been deployed).

[12] The five gliders used in the experiment were positioned in a two-dimensional array in the Philippine Sea from 8 to 17 May, 2004. The central node, at 20° N, 129° E, was surrounded by four others located half a degree away in each of the cardinal directions (Figure 1). The study area, approximately 800 km east of Luzon Strait in the western tropical Pacific, is located in depths of 5000–6000 m well offshore of the Kuroshio, the dominant regional surface current. Upper-ocean currents in the area are dominated by tidal motions and energetic westward-propagating mesoscale eddies. The size of the array, roughly a 100-km square, was chosen to capture the mesoscale variability associated with these eddies.

[13] Each vehicle repetitively profiled from just below the surface to 200 m depth while attempting to hold station at a fixed geographic position. The actual three-dimensional vehicle trajectory often resembled a skewed helix due to

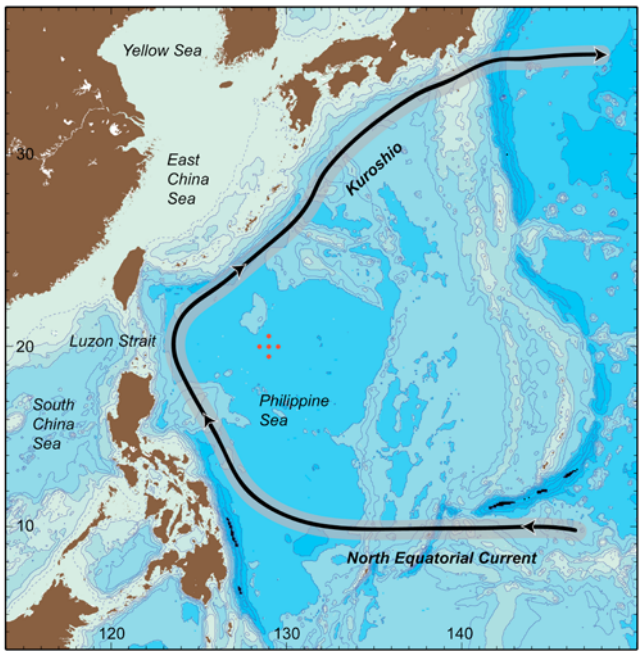

Figure 1. The study area, located in the central Philippine Sea, approximately 800 km east of Luzon Strait in the western tropical Pacific. The dominant regional surface current, the Kuroshio, passes to the east and north of the study site. Nominal measurement locations are marked with red dots. Bathymetry contour spacing is 1000 m.

the glider's finite turning radius and local ocean currents (Figure 2). The resulting time series measurements at each array node, including CTD/optical profiles every 40 minutes and slab velocity estimates every 2 hours, are interpreted

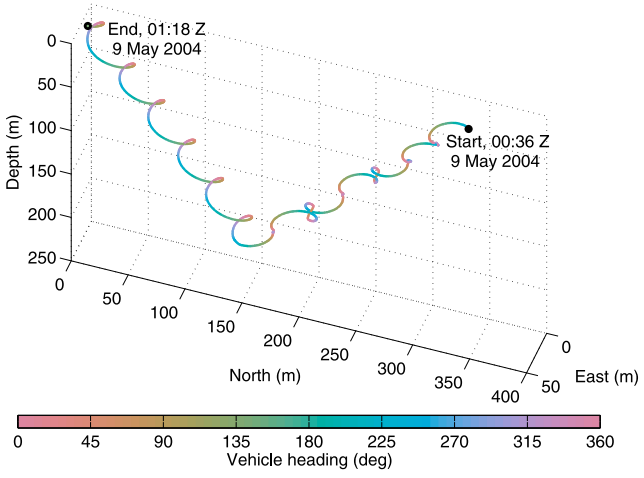

Figure 2. The underwater trajectory, during a single dive, of a glider attempting to hold station at the western node of the array. During this dive, the dead-reckoning calculations made by the glider indicated that it was looping around the station location, but the local current was actually carrying it steadily southward (right to left in the diagram). After a few more dives, the glider surfaced to the south of the intended location, obtained a GPS fix, and proceeded northward, back toward the station. The trajectory was reconstructed assuming a steady, vertically uniform current.

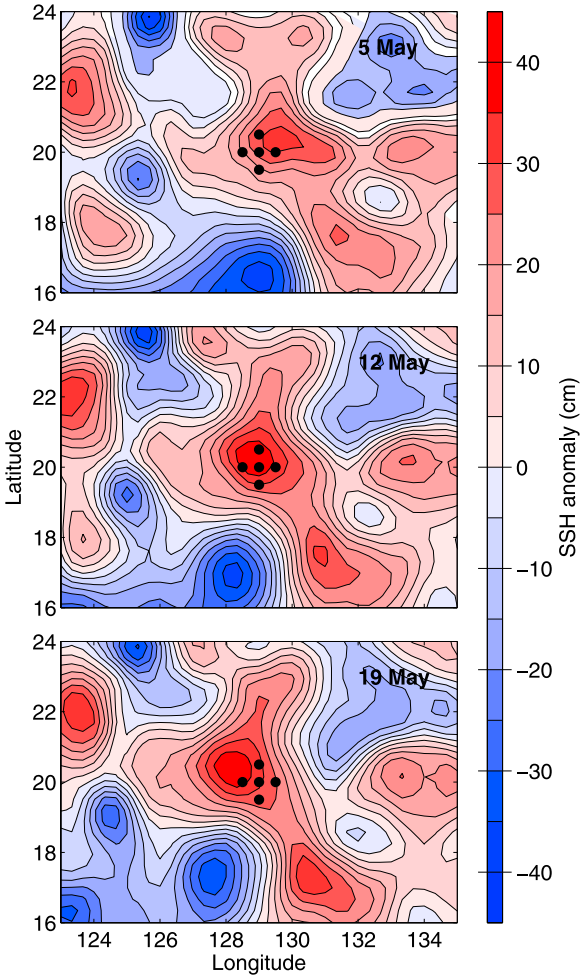

Figure 3. Dynamic height in the vicinity of the array calculated from Jason, TOPEX/Poseidon, and ERS altimetry (data obtained from AVISO): (top) 5 May 2004, (middle) 12 May, (bottom) 19 May. Note the anticyclonic eddy (red feature near the middle of the panels) propagating westward through the study area.

below in the same manner as a physically moored chain of instruments would be.

2.3. Data Processing

[14] Raw time series of temperature, conductivity, pressure, and chlorophyll fluorescence collected on the descending legs of each dive were processed with a three-point median filter to reject obvious outliers. The time series were then converted to quasivertical profiles using the CTD pressure as the independent coordinate, and each profile was indexed by its median time and position. The resulting profiles (approximately 1400 total) were then treated in a manner analogous to shipboard hydrographic data. At an ascent/descent angle of 25° from the horizontal, the distance traveled during one profile is approximately twice the dive depth, or 400 m in this application. The potential position error made during this transformation is equivalent to drift of approximately two ship lengths (200 m) during a 40-minute hydrographic cast.

[15] Salinity was computed from temperature, pressure, and conductivity using standard methods. Factory-supplied

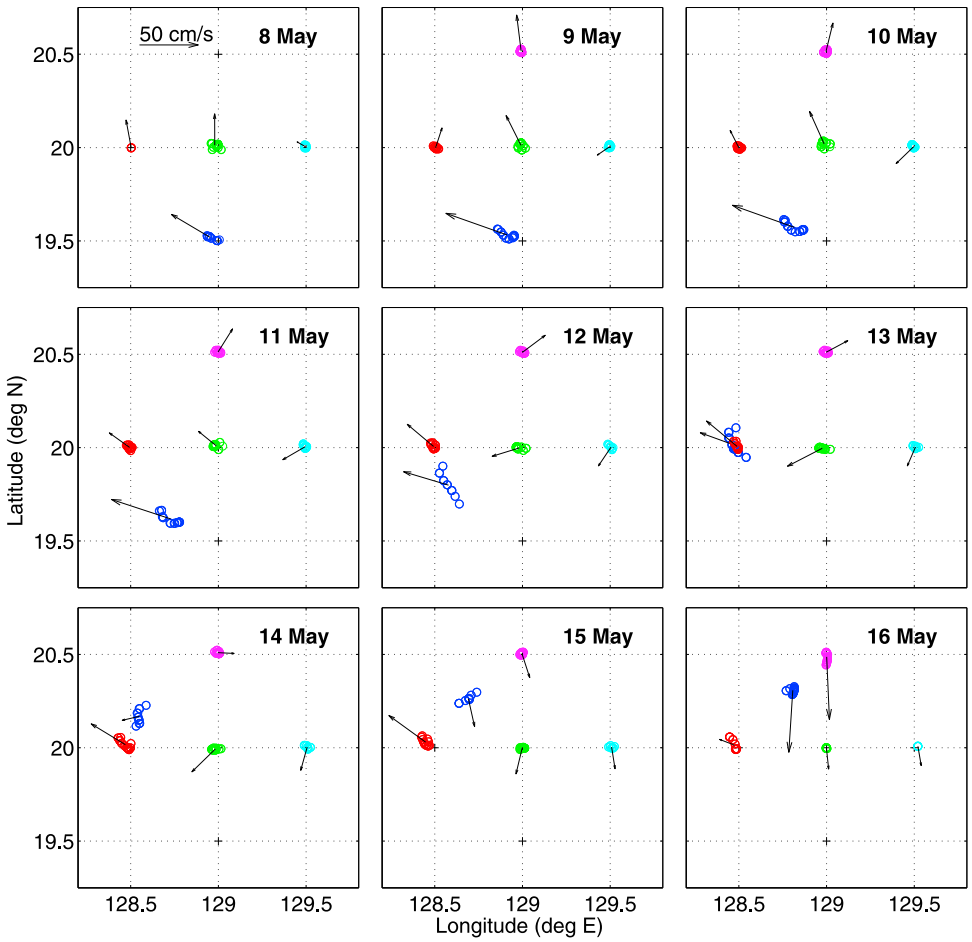

Figure 4. Locations of the gliders and inferred upper 200-m slab velocities during the experiment. Each panel represents a 24-hour period; all the surface position fixes obtained during that time interval are plotted as colored circles. The target position of each glider is marked with a black cross. The corresponding 24-hour mean inferred slab velocities are plotted as arrows with bases located at the time average of each glider's position during the interval. Averaging velocity measurements suppresses tidal variability. The glider originally stationed at the southern node of the array (dark blue circles) was unable to hold station and was reprogrammed on 11 May to circumnavigate the array. The clockwise circulation of an eddy is apparent throughout. Early in the deployment the current over most of the array is northward; by the end, the center of the eddy had reached the western side of the array, and the current was predominantly southward.

calibrations were applied to the WET Labs ECO-bb2f data to convert raw counts to chlorophyll (mg/m^3). In the absence of accurate chlorophyll measurements at this location the prescribed linear scaling is somewhat arbitrary. The following results and conclusions depend only on the spatial and temporal structure of the chlorophyll fluorescence measurements and not on the actual measured chlorophyll concentrations.

3. Currents and Station Holding Performance

[16] During the experiment, an anticyclonic eddy, visible in satellite altimetry (Figure 3) was moving through the study area. The eddy was approximately centered over the array location on 12 May (near the midpoint of the deployment period; Figure 3, middle).

[17] On timescales longer than a day, the flow associated with this feature dominated the 0–200 m average current velocity recorded by the gliders; in the sequence of daily maps of glider locations and average slab velocities (Figure 4), the flow evolves from northward (eddy to the east) to clockwise rotation (eddy coincident with the array) to southward (eddy to the west). GPS fixes (and therefore current velocity estimates) were obtained by each glider at about 2.5-hour intervals; the positions measured during the approximately 10 periods when each glider came to the surface each day are plotted in the corresponding panel, with a different color for every glider. The slab velocity estimates corresponding to these positions are averaged together; the resulting daily mean current velocities for each glider are plotted as black arrows. The 24-hour average suppresses strong velocity fluctuations due to the tide.

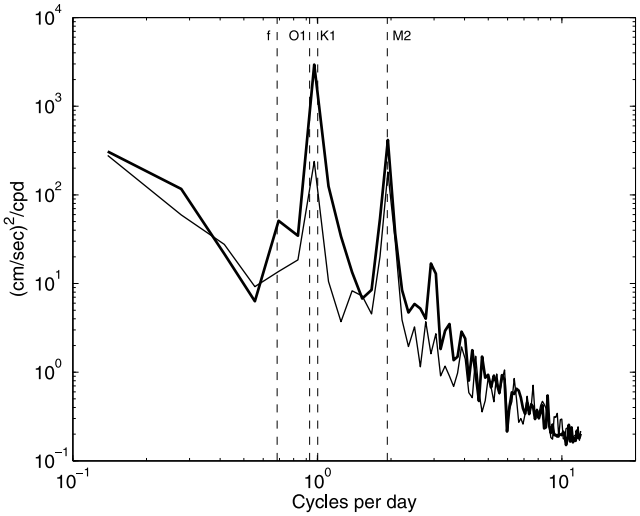

Figure 5. Rotary spectra of 0–200 m slab velocities measured by all five gliders during the entire deployment. The clockwise component is plotted as a bold line and the counterclockwise component as a thin line. Frequencies of three tidal constituents (the lunar semidiurnal M2, the solar diurnal O1, and the luni-solar declinational diurnal K1) are marked, as is the inertial frequency, *f*. Strong clockwise-rotating diurnal tidal velocities were observed at all stations.

[18] At the southern station, the flow associated with the anticyclonic eddy passing through the array combined with that of an intense cyclonic eddy centered a few hundred kilometers to the south (blue feature at the bottom of each panel in Figure 3), creating strong currents that carried the southern glider west and north off station early in the deployment. The estimated 0–200 meter depth-averaged current velocity varied from 30 to 75 cm/sec. Three days into the deployment, it became clear that the vehicle, 30 km downstream from its target, would not readily regain the station, and on 11 May, the southern glider was reprogrammed to fly clockwise around the perimeter of the array.

[19] On timescales shorter than a day, semidiurnal and especially diurnal tidal motions dominated local currents. The dominant feature in the rotary spectrum of slab velocity formed from measurements made by all five gliders (Figure 5) is the peak in the clockwise power near the frequency of the K1 diurnal tidal constituent. Strong, clockwise-rotating diurnal velocity variations were recorded independently by all of the vehicles. As discussed in the following section, the baroclinic motions of the associated diurnal internal tides were a primary source of variability in the time series of physical and bio-optical seawater properties.

[20] In spite of the substantial flows associated with the eddy and the strong tidal variability, which made it difficult to accurately predict and compensate for the prevailing currents, four of the five vehicles were able to hold station effectively. The size of the effective watch circle varied from vehicle to vehicle (Figure 6), with the eastern and northern vehicles outperforming those at the center and western stations, but all four maintained an RMS distance from the desired location of less than 4 km. This station-holding performance is comparable to the watch circle expected from a bottom-moored surface mooring in similar (6000 m) water depth (R. Weller, personal communication, 2005) and is adequate for most oceanographic analyses.

4. Results and Discussion

[21] Although organized primarily as a demonstration of glider capabilities, this field exercise provides a unique data set for examining biological-physical interactions in the open ocean. With spatially distributed time series of both physical and bio-optical seawater properties, measured with fine vertical resolution, it is possible to follow the movement in space and development over time of thin biological features, and to frame those changes within the physical context of their environment.

[22] Much of the variability observed in the time series (Figure 7) is associated with semidiurnal and diurnal internal tides. Perhaps most obvious in the oscillations in the depth of the deep chlorophyll maximum (bottom row in the figure), the waves are also apparent in the physical properties; the tidal oscillations driving the waves are visible as well (stick plots of slab velocity at the top of the figure). Analyzing the chlorophyll time series using potential density as the vertical coordinate rather than depth (Figure 8) conceals the effect of simple vertical advection by these internal waves on the vertical structure, allowing us to focus on other processes.

[23] With the isopycnal heaving associated with diurnal internal tides removed, other daily cycles in the concentration of chlorophyll are still apparent. The gross structure of the chlorophyll field is constant: a strong persistent deep chlorophyll maximum (DCM) was observed by all five vehicles throughout the deployment at a potential density (σ_θ) of approximately 23.3 kg/m^3, corresponding to an

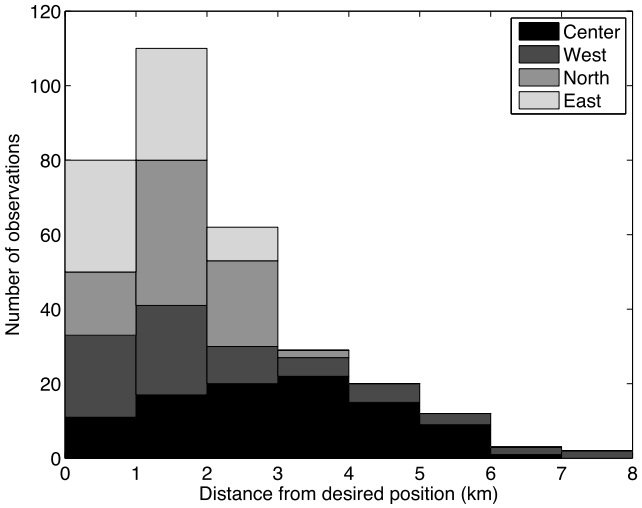

Figure 6. Stacked histograms of surface position fixes by distance from the desired location, indicating the station-holding performance of the four successful synthetic moorings. Each bar of the histogram is divided into bands, which are shaded, to distinguish between the four vehicles. The glider at the eastern station never strayed as far as 3 km from its station, while the one at the northern station reached as far as 8 km; all four vehicles maintained an RMS distance from station of less than 4 km.

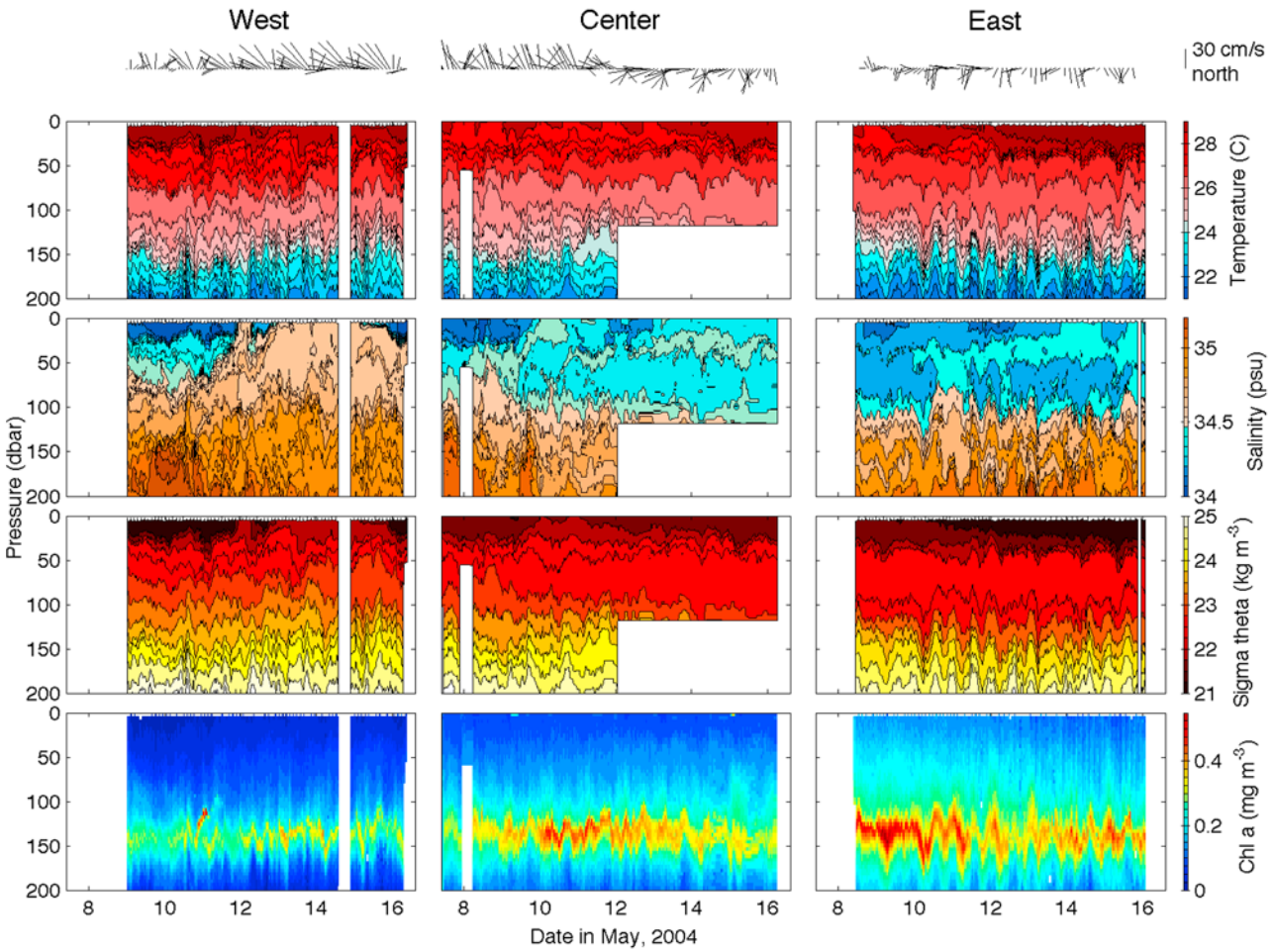

Figure 7. Time series of (top) temperature, salinity, potential density, and (bottom) chlorophyll fluorescence from the (left) western, (center) center, and (right) eastern stations. Slab current velocities are shown as stick plots above each column. Note the switch from northward to southward average currents at the center station when the eddy passed over it midway through the deployment. White areas denote missing data.

average depth of approximately 140 m. Near the surface, however, especially at the northern station (Figure 8, top), measured fluorescence is notably lower during the middle of the day than at other times; we attribute this signature to fluorescence quenching, which is known to occur in brightly lit surface waters [e.g., *Krause and Weis*, 1991; *Falkowski and Kolber*, 1995]. Deeper in the water column, in the vicinity of the DCM, the diurnal cycle is out of phase with the quenching cycle at the surface: it is retarded by 90 degrees (6 hours), with maximum chlorophyll concentrations occurring near sunset and minimum concentrations at dawn. Zooplankton distributions were not measured, making grazing of phytoplankton difficult to estimate, but we hypothesize that the deep daily cycle in chlorophyll is driven by phytoplankton growth, which causes chlorophyll concentration to increase during daylight hours. This growth is offset by respiration, death, and grazing, which combine to reduce the chlorophyll concentration at night, but are outstripped by growth during the day.

[24] Against the background of the diurnally pulsating but essentially steady DCM, certain features stand out. In particular, a thin region of high chlorophyll concentration is apparent at a potential density near 23 kg/m^3 (just above the DCM), at the western station around 11 May (Figure 7, bottom left and Figure 8, left). A few hours later, a similar short-lived feature appeared at the northern station (Figure 8, top). The synchronization of the two events and the fact that both features occur in water of the same density strongly suggest that, though separated by some 75 km, they represent two arms of the same high-chlorophyll layer.

[25] The water forming the high-chlorophyll feature is low in salinity, suggesting that a pocket of fresh water experienced a minibloom, which was then advected horizontally across the array. Harder to pick out in the time series of salinity from the northern station (Figure 9, top), the feature appears clearly near a potential density of 23 kg m^{-3} on 11 May as a fresh layer at the western station (Figure 9, left). The evolution of the feature and the correlation between chlorophyll fluorescence and salinity is clearer in the sequence of individual profiles (Figure 10). At the western station (Figure 10, middle) the feature appears at approximately 19:00 GMT on 10 May, initially 20 m thick, and gradually grows thinner over the course of the following 12 hours forming a thin layer with a thickness

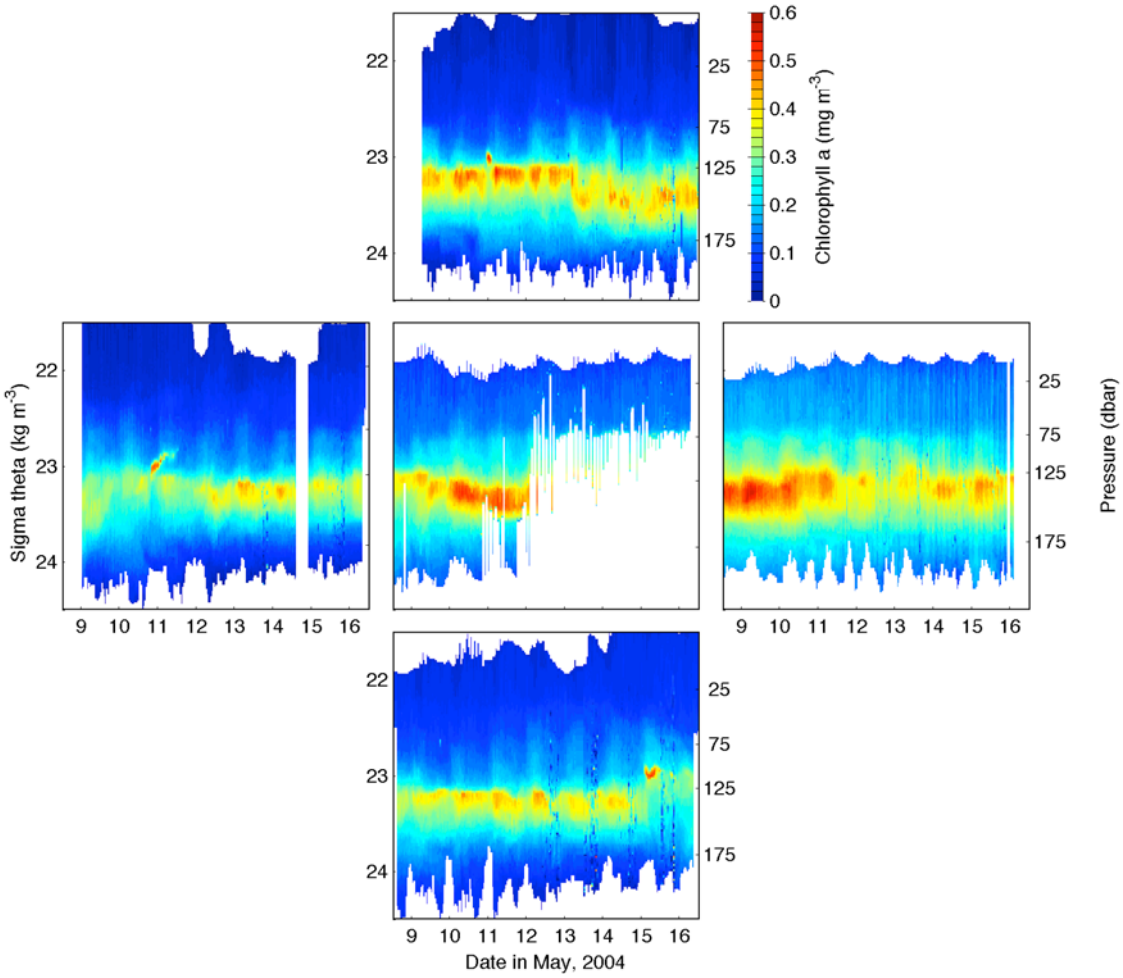

Figure 8. Chlorophyll *a* fluorescence recorded by each of the vehicles. Panel locations correspond to array nodes, with north up. Vertical coordinate is potential density rather than depth, concealing substantial diurnal isopycnal heaving. The average densities at four different depths are marked on the right-hand side of each panel. Missing data from the center station is due to a malfunctioning temperature sensor. Chlorophyll concentrations reported here are based on factory calibrations of the fluorometers and are nominal only.

of less than 3 m. Example profiles of chlorophyll and salinity taken toward the end of the thinning process, drawn in bold in Figure 10, are expanded in Figure 11 to show detail, together with the profile of potential temperature.

[26] At the northern station (Figure 10, top), the high-chlorophyll feature first appears at approximately 23:00, 4 hours behind the western station. As in the observations from the western station, it begins to grow thinner, slimming from an initial thickness of 25 meters over the course of 3 hours, but then it disappears, presumably advected away from the array node by prevailing currents, having reached a minimum thickness of approximately 12 meters.

[27] At both locations, though more obviously at the western station where the salinity signature is more pronounced, the thinning occurs identically in the profiles of chlorophyll (green) and salinity (blue), indicating that the thinning process, in this case, is driven by physical forcing, as opposed to a biological mechanism such as convergent swimming or spatial variation in growth rate. Therefore in the investigation of the cause of the thinning of the phytoplankton layer, chlorophyll may safely be treated as a conservative tracer (this is not true in the context of the formation of the high-chlorophyll feature in the first place, a question which we sidestep here).

[28] Because the feature was located below the base of the mixed layer where the diffusivity is small, and because the thinning occurred relatively rapidly, we make the further assumption that the effects of diffusion can be neglected. For the purposes of analyzing the thinning of the preexisting feature, then, we have:

$$\frac{DC}{Dt} = \frac{\partial C}{\partial t} + \mathbf{u} \cdot \nabla C = 0 \tag{1}$$

Here and throughout this section, variables are defined as described in Table 1.

[29] In order for a horizontal layer of chlorophyll to grow thinner without decaying in intensity, the vertical gradient of the chlorophyll concentration must increase. Differentiating the equation (1) with respect to z, we obtain an expression

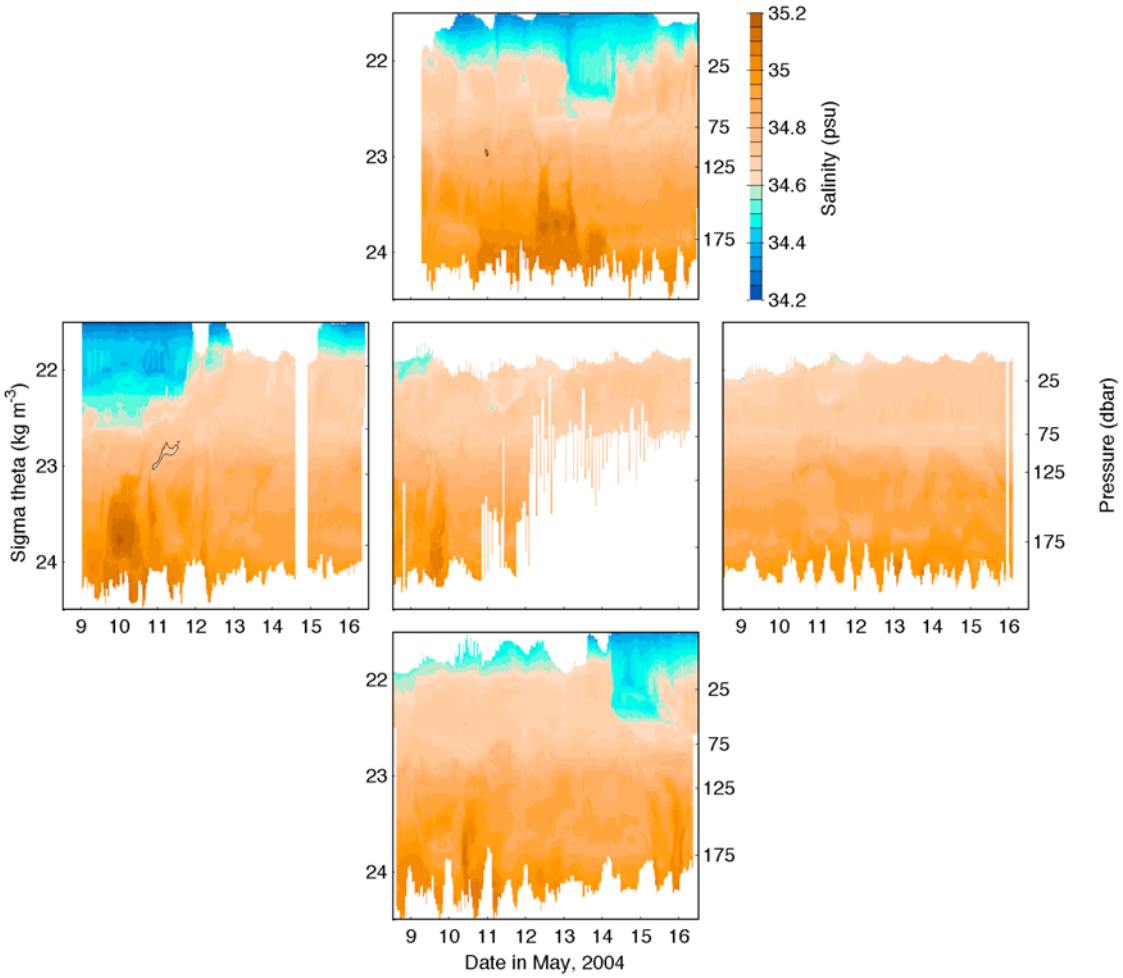

Figure 9. Salinity measured by each vehicle, plotted as in Figure 8. Black lines are domain-limited contours outlining low-salinity features. These features have high chlorophyll concentrations (Figure 8). Contour levels are 34.79 psu (top) and 34.71 psu (left).

for the time rate of change of the vertical gradient of chlorophyll concentration following a material element:

$$\frac{D}{Dt}\left(\frac{\partial C}{\partial t}\right) = -\frac{\partial \mathbf{u}}{\partial z}\cdot\nabla C = -\frac{\partial w}{\partial z}\frac{\partial C}{\partial z} - \frac{\partial \mathbf{u}_{\mathrm{H}}}{\partial z}\cdot\nabla_{\mathrm{H}} C \qquad (2)$$

[30] We have split the right-hand side of equation (2) into two terms. The first involves the vertical strain: the rate of change of the vertical velocity, w, with vertical distance, z; the second involves vertical shear: the rate of change of horizontal velocity with z (the subscript H in the velocity vector and the gradient operator stands for "horizontal" – no z component). These two mechanisms affecting vertical gradients of tracers in a fluid are well known [e.g., *Eckart*, 1948; *Franks*, 1995; *Birch et al.*, 2008]: negative vertical strain (vertical convergence) enhances an existing vertical gradient, and vertical shear of a horizontal gradient creates a vertical gradient that increases over time. A layer thinned by the former mechanism, i.e., by the pinching together of isopycnals, would not grow thinner in density space. The thinning observed in Figure 10 (bottom), then, is an indication that vertical strain alone cannot explain the formation of the thin layer; we must consider the influence in equation (2) of the shear term $-\frac{\partial \mathbf{u_H}}{\partial z}\cdot\nabla_{\mathbf{H}} C$.

[31] The appearance of the horizontal concentration gradient in this shear term reflects the fact that in the absence of horizontal structure in the concentration of chlorophyll, vertical shear has no influence at all on the chlorophyll field: an infinite uniform layer of phytoplankton parallel to the streamlines of the flow, for example, is unaffected. As flow in the ocean occurs primarily along isopycnals, a tracer whose concentration varies along isopycnals is susceptible to thinning by shear. A thin layer formed in this manner slants across isopycnals. During the course of the thinning process, the potential density at the layer observed at the western station decreased from 23 to 22.9 kg/m^3 (Figure 10, bottom), consistent with a slanted layer being thinned by shear as it is advected past the measurement site.

[32] The influence of such advection has been hidden in the Lagrangian derivative (left-hand side of equations (1) and (2)) in the above description of the evolution of the vertical gradient of a passive tracer. This was done in order to emphasize the mechanisms that cause thin layers to form: pure advection by a uniform flow does not form thin layers –

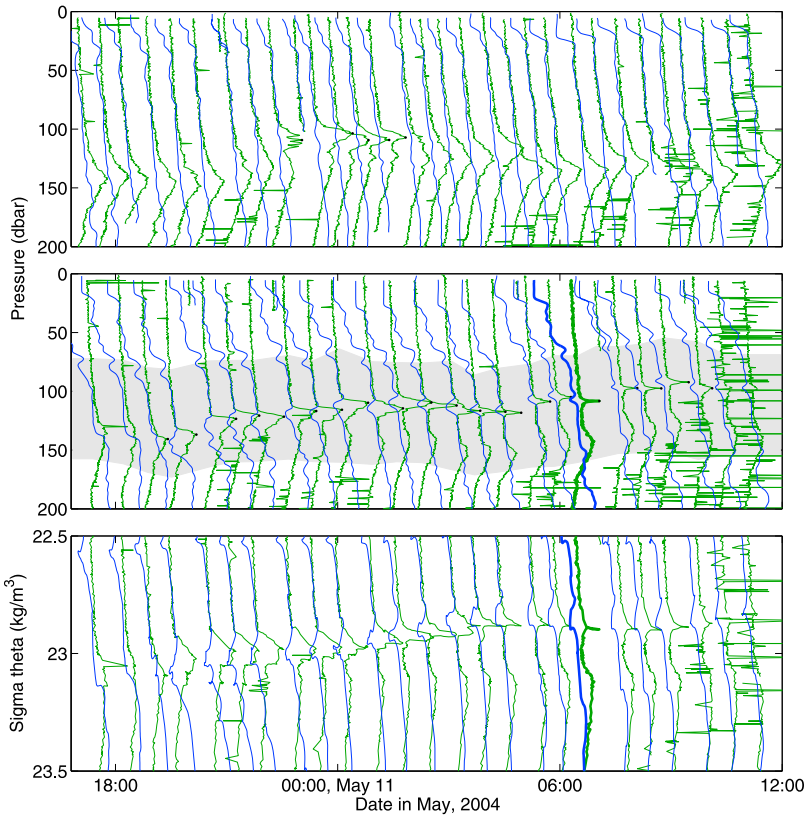

Figure 10. Waterfall plot of chlorophyll fluorescence (green) and salinity (blue) during the formation of a thin phytoplankton layer at the western station. (top) Northern station; (middle) western station; the area between the 22.5 and 23.5 kg/m^3 isopycnals is shaded, indicating the domain shown in the bottom; (bottom) the profiles from the western station replotted, with density as the vertical coordinate. Thick lines in the lower two panels mark profiles expanded in Figure 11. The horizontal axes measure time in hours, with profiles, plotted in arbitrary units, centered over the time they were measured. Note the inverse relationship between chlorophyll and salinity in the region of the thin layer.

it only transports them. However, the observations presented here were not made by a platform that follows the flow making measurements in the vicinity of a particular fluid element, as isolation of those formation mechanisms would have required. Instead, each vehicle attempted to profile repeatedly in the same location, yielding nearly Eulerian time series. Although accurate estimation of the velocity with which the seawater making up the high-chlorophyll layer flowed past the glider station is not possible – vertical current structure was not measured and the array was too coarse to capture the propagation of small-scale features – it is likely that the layer was subject to both vertical shear and a nonzero mean current as it was observed.

[33] *Birch et al.* [2008] provide a simple model with an analytic solution for a patch of plankton thinned by shear: the initial concentration is a two-dimensional (vertical and one horizontal dimension) Gaussian patch, and the flow is a simple shear. For the purpose of illustrating the combined effect of shear and advection on the evolution of the vertical profile of a patch as measured in a single location, we employ their model, modifying the initial conditions slightly such that the current velocity at the center of the patch is nonzero, and, for simplicity and because we are interested in timescales much smaller than the vertical diffusion time, omitting the effect of diffusion. The flow is a simple shear: the x, y, and z components of the fluid velocity are $u = \alpha z$, $v = 0$, and $w = 0$. The initial distribution of chlorophyll, arbitrarily normalized such that the maximum concentration is 1, is given by:

$$C(x,z,0) = \exp\left(-\frac{(x-x_0)^2}{2L_0^2} - \frac{(z-z_0)^2}{2H_0^2}\right) \qquad (3)$$

where x and z, the horizontal and vertical coordinates, are defined to be zero at the horizontal location of an imaginary mooring and the vertical level at which the flow velocity is zero, respectively. In the example presented here (Figure 12) the initial horizontal location of the center of the patch, x_0, is -600 m, and its vertical location, z_0, is -25 m. The initial horizontal length scale of the patch, L_0, is 100 m, and the initial vertical length scale, H_0, is 10 m. The vertical shear, α, is -10^{-3} s^{-1}. The vertical domain depicted in each frame of Figure 12 ranges from $z = 0$ to $z = -50$ m, but to facilitate comparison with other figures, the vertical axes are labeled as density rather than depth, assuming a uniform vertical stratification $\partial\rho/\partial z$ of -10^{-2} kg m^{-4}. The layer, as observed at $x = 0$ (the location in the model domain at which we imagine a mooring), grows thinner with time and moves

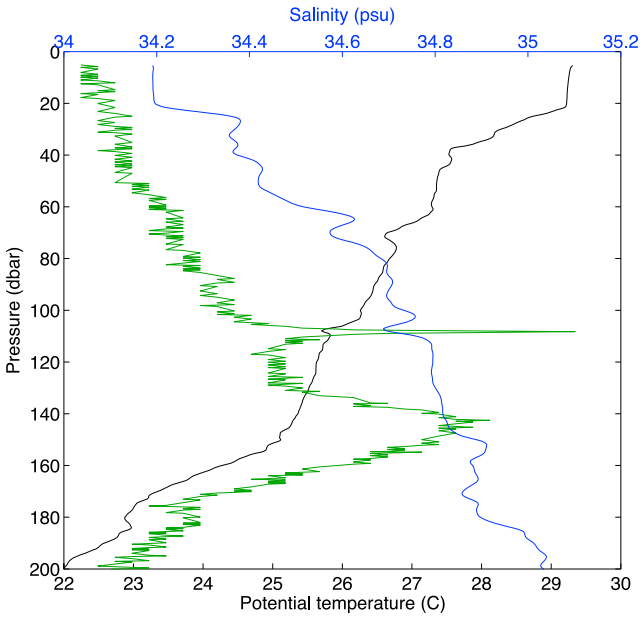

Figure 11. Profiles of potential temperature (black), salinity (blue), and chlorophyll fluorescence (green) recorded at the western station at 06:30 GMT on 11 May 2004. The chlorophyll and salinity profiles shown in detail here are drawn as bold lines in Figure 10. The range spanned by the horizontal chlorophyll axis (not shown) is 0–0.5 mg/m^3.

into water of lower density. The evolution of the profile of chlorophyll at this location in the model is reminiscent of that actually observed by the synthetic mooring at the western station (Figure 13).

[34] The parameter values in the illustrative model were chosen to roughly optimize that similarity in the rates of thinning and density shift, but many other parameter combinations would work equally well. For example, Figure 13 (top) would be unchanged if L_0, x_0, and α were all changed by the same multiplicative factor. The overall size of the high-chlorophyll layer was much larger than the 100 m horizontal length scale chosen in the model, as it was observed simultaneously at synthetic mooring stations separated by 75 km. This may seem to indicate that increasing the values of the above parameters would result in a more realistic approximation of the actual conditions. However, the relevant length scale is not the overall horizontal extent of the layer, or even the overall extent before shearing, but rather the scale of horizontal structure within the layer. Moreover, we hesitate to hypothesize much stronger vertical shear: the large values of vertical shear that probably contribute to the formation of many thin biological layers in coastal environments are less likely to occur within the open ocean thermocline. The suggestion, in any case, is a patchy layer of enhanced chlorophyll concentration being thinned by shear as it advects through the synthetic moored array.

[35] Direct measurements of vertical shear were not made at the glider stations during the formation of the thin layer. However, by comparing simultaneous density profiles form different nodes of the array, we can estimate the geostrophic shear between them. Midway through the deployment, the temperature sensor on the glider at the center station began to malfunction, and the glider assigned to the southern node was unable to hold station. From the other three stations, however, density differences between approximately orthogonal pairs of points can be calculated for the full deployment. Although scaled in Figure 14 as geostrophic shear, the dominant signal which emerges is that of diurnal internal waves rather than steady, geostrophyically balanced shear. The density difference between water at the northern station and that at corresponding depths at the eastern and western stations changes sign periodically, completing one cycle per day, with the cycle on the western side slightly lagging the one on the eastern side. Near the middle of the record, upward phase propagation of the waves can be discerned.

[36] *Franks* [1995] put forward near-inertial internal wave shear as a likely mechanism for the formation of thin layers. Estimation of the magnitude of the vertical shear associated with the waves we observed is difficult, as their wavelength is not well known, but the horizontal density gradients on ~100 km scales (Figure 14) suggest a lower bound of 10^{-3} s^{-1}. This is the value used in the simple shear model above, and it is typical of vertical shear associated with low-frequency internal waves in the upper open ocean [*Gargett et al.*, 1981].

[37] A second source of shear, aside from low-frequency internal waves, is steady geostrophic flow. We apply a running mean of one inertial period (~35 hours) to the calculated geostrophic shear components (shown in Figure 14), which filters out most of the influence of internal waves, and then combine the two nearly orthogonal components to form an estimate of the total geostrophic shear within the array. From this estimate, we calculate the mean square geostrophic shear profile for the entire deployment (Figure 15). The shear profile has a peak in the same density range as the DCM (the chlorophyll profile in Figure 15 is a full-deployment average in density space from the west, north, and east stations), but the thin layer observed at the western station occurred somewhat shallower, at a potential density near 23 kg m^{-3}, where the mean geostrophic shear is smaller.

[38] Forming a shear magnitude estimate from the geostrophic shear components from two different locations (between the east and north stations and between the north and west) as if they applied to the same location is a

Table 1. Variable Definitions

Variable	Meaning	Unit
C	chlorophyll concentration	arbitrary units
t	time	s
x	zonal spatial coordinate	m
y	meridional spatial coordinate	m
z	vertical spatial coordinate	m
$\mathbf{u}$	water velocity	m/s
u	x component of velocity	m/s
v	y component of velocity	m/s
w	z component of velocity	m/s
L	horizontal patch lengthscale	m
H	vertical patch lengthscale	m
α	vertical shear	s^{-1}
ρ	water density	kg/m^3
0 (subscript)	initial value	
H (subscript)	horizontal	

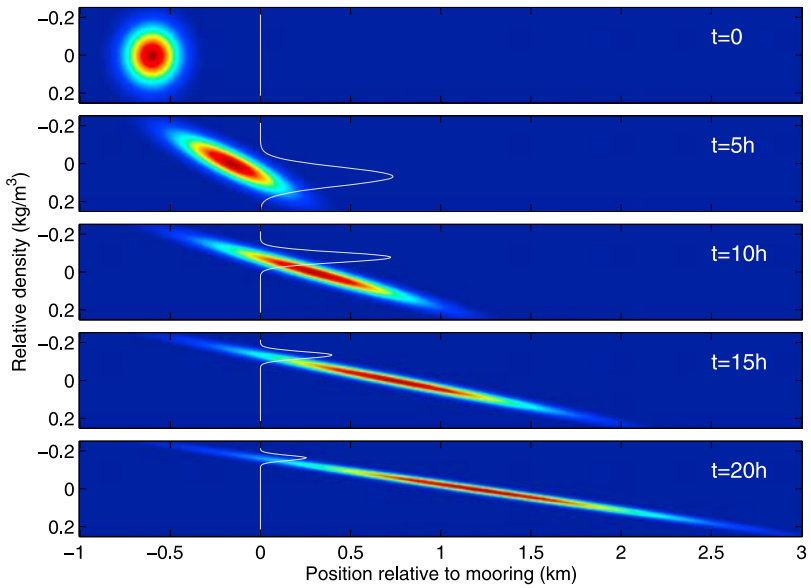

Figure 12. Modeled evolution of a Gaussian plankton patch, at 5-hour intervals from $t = 0$ to 20 hours, under the influence of steady, uniform vertical shear with a magnitude of 10^{-3} s^{-1} [see *Birch et al.*, 2008]. Profiles at the location of a hypothetical mooring are drawn in white. The vertical axes are labeled in density; the uniform vertical stratification is -10^{-2} kg m^{-4}. The initial horizontal and vertical length scales of the patch are $L_0 = 100$ m and $H_0 = 10$ m, respectively. The chlorophyll concentration scale is arbitrary; the sequence of colors is identical to that shown in the color scale of Figure 13.

possible source of error, but the location of the maximum shear layer is insensitive to variations in the calculation: it appears at approximately the same density in shear calculated from all 10 pairs that can be formed from the 5 stations. The shape of the shear profile (Figure 15) is fairly robust. Although geostrophically balanced flow may have played a role in the formation of the thin layer, the shear associated with diurnal internal waves was probably larger.

5. Conclusions

[39] 1. The synthetic moored array was shown to provide an efficient means for a single survey ship to rapidly obtain

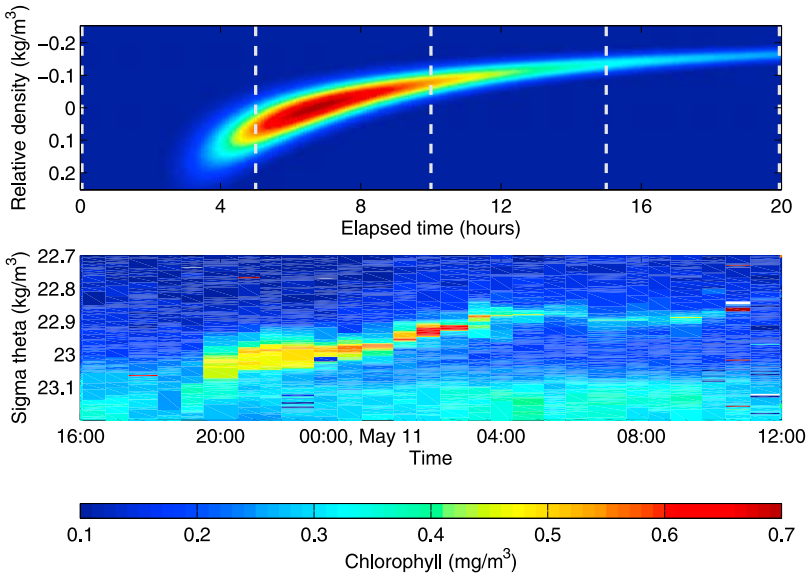

Figure 13. Time evolution of the vertical profile at a single horizontal location of a high-chlorophyll layer. (top) Chlorophyll concentration at $x = 0$ in the simple shear plus advection model; the 5-hour intervals marked with white dotted lines correspond to the snapshots shown in Figure 12. (bottom) Measurements made at the western station of the array. The vertical coordinate is density, eliminating the visual impact of vertical advection; note the variation in the density at the center of the layer.

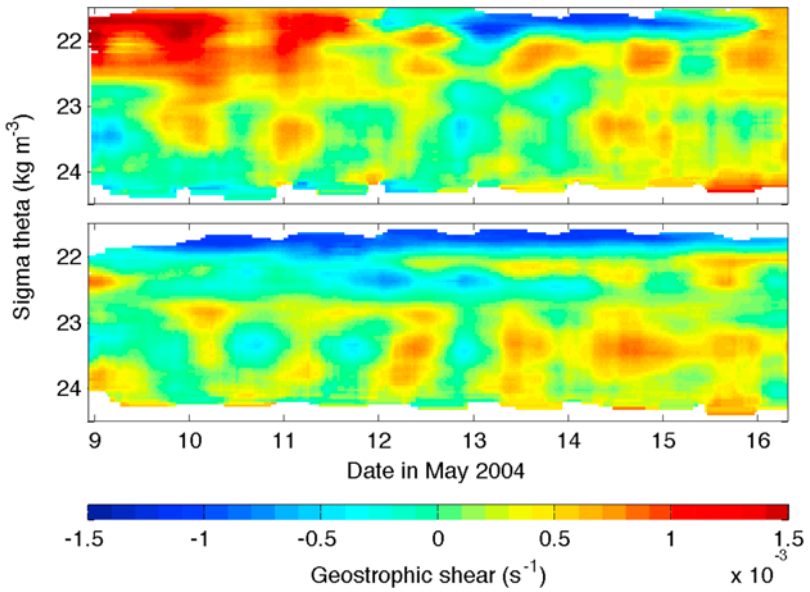

Figure 14. Simultaneous differences in potential density at corresponding depths between (top) the western and northern stations and (bottom) the northern and eastern stations. The density difference at each depth and time was mapped into density space using the mean density at the two stations at that depth and time. The result was smoothed with a 12-hour running mean. Positive values indicate higher density at the northern station, i.e., southeastward geostrophic shear in the top and northeastward in the bottom. Note the strong diurnal signal, the upward phase propagation near the middle of the record, and the temporal lag between the two cycles.

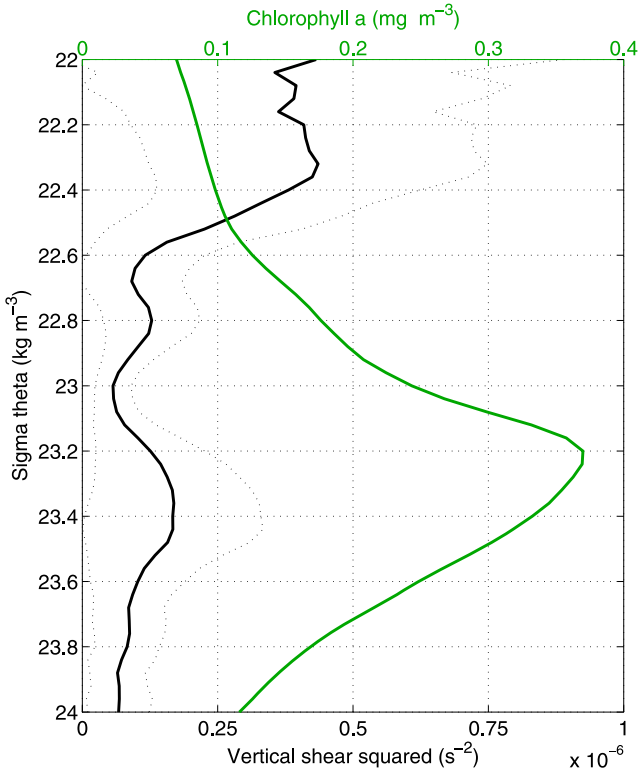

Figure 15. Full-deployment mean square geostrophic shear and chlorophyll concentration as functions of density. Geostrophic shear components were calculated as in Figure 14, but smoothed with a longer, 35-hour running mean to filter out the contribution of internal waves. The solid black line is the mean of this geostrophic shear squared; dotted lines indicate plus and minus one standard deviation. The average chlorophyll profile (green line) was calculated in density space from all the profiles measured at the northern, western, and eastern stations.

spatially distributed, vertically dense time series data at low cost and with minimal need for on-site technical support. While the stability of the array was generally adequate, gliders with greater operational depth will be more effective at holding station in tropical regions characterized by strong, surface-intensified currents.

[40] 2. Temperature, salinity, and velocity time series from all vehicles exhibit pronounced semidiurnal and especially diurnal fluctuations associated with the internal tide. Maximum isopycnal displacements exceeding 40 m are observed near 150 m depth. Related variability is also evident in the deep chlorophyll maximum near 130–140 m.

[41] 3. A cool, fresh, high-chlorophyll layer was observed over a 14-hour period, during which time it gradually thinned from approximately 20 m to a minimum thickness of approximately 2 m. The evolution of this feature, both its thinning and its migration upward across isopycnals, was consistent with the action of shear, most likely associated with diurnal internal waves, combined with advection.

Appendix A

[42] The optical measurements made during the experiment were plagued by intermittent noise (see the profiles of fluorescence in Figure 10). This appendix is an explanation of the source of that noise.

[43] The noise occurred at all stations, and worsened as the deployment progressed. It occurred only at night, and began earlier in the evening at deeper depths than in shallower ones (see, for example, Figure 10, top), suggesting that ambient light was a factor.

[44] Upon recovery of the gliders, many small driftfish, (G. Allen, personal communication, 2008), possibly *Psenes cyanophrys*, approximately 4 cm in length, were found dead in the flooded tail cones (Figure A1). Apparently attracted to the flashing optical sensor, which acted as a beacon in the dark, they continually swam in front of the sensor, seriously

Figure A1. Driftfish (possibly *Psenes cyanophrys*) found trapped in the tailcone of a glider. The fish were so abundant in the vicinity of the gliders at night that they interfered with the function of the chlorophyll fluorometers, dominated the optical backscatter signal, and slowed the vehicles down by up to 50%.

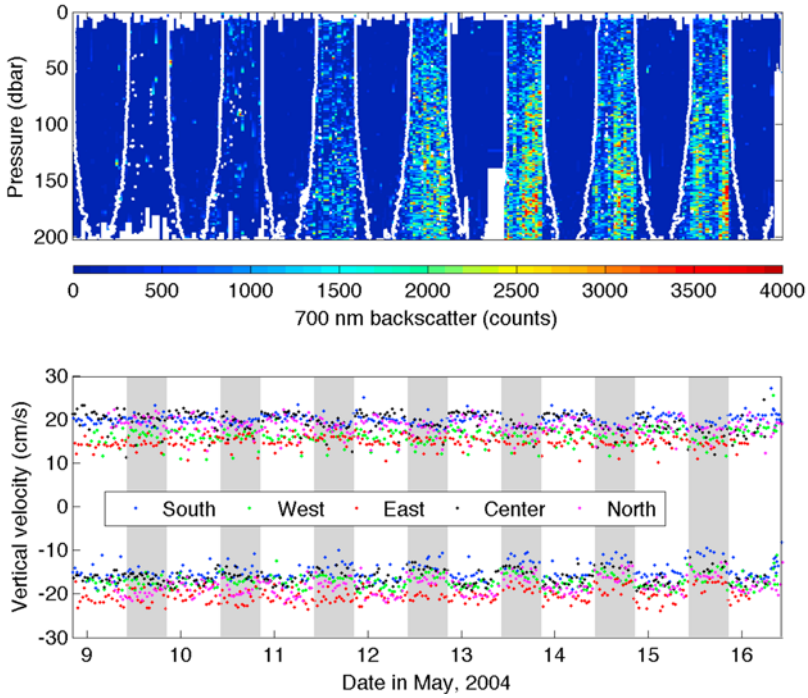

Figure A2. (top) 700-nm optical backscatter measured by the glider originally assigned to the southern station (backscatter records from the other vehicles are similar). White lines are contours of PAR at a level of 10^{-4} relative to surface midday values. (bottom) Vertical vehicle velocity. Two points are plotted for each dive of each glider: one is the average vertical velocity during the ascent and the other is the average vertical velocity during the descent. Gray bars indicate night. Note the diurnal variations, increasing over the course of the deployment, in both optical noise and vertical vehicle velocity.

degrading the quality of the nighttime fluorescence and optical backscatter data.

[45] The fish had a further impact on the gliders as well: at the same times when optical data was noisy—at night and during the second half of the deployment (Figure A2, top)—the velocity of the gliders through the water was decreased by up to 50 % on both ascents and descents, corresponding to roughly a doubling of the vehicle drag coefficient (Figure A2, bottom). The mechanism behind the slowing is not known. The turbulence caused by the movement of the fish may increase the drag experienced by the vehicle, or the fish may physically touch the glider, hitching a ride and so roughening its streamlined surface.

[46] **Acknowledgments.** This program was organized as a demonstration of glider capabilities for the Naval Oceanographic Office. We acknowledge the assistance of Robert Lorens (NAVO) and Tom Curtin (ONR) in facilitating this program. The Office of Naval Research provided support for fieldwork and analysis through grants N-00014-00-1-0256 and N-00014-05-1-0367. We thank the captain and crew of the *USNS Heezen* for their able assistance at sea. The success of this program reflects the care taken by John Lund during instrument preparation, deployment, and recovery. We thank Terri Paluszkiewicz (ONR) for support enabling the publication of these results.

References

Bellingham, J. G., and J. S. Willcox (1996), Optimizing AUV oceanographic surveys, in *Proc. of the 1996 Symp. on Autonomous Underwater Vehicle Technology*, pp. 391–398, IEEE, Piscataway, NJ.

Birch, D. A., W. R. Young, and P. J. S. Franks (2008), Thin layers of plankton: Formation by shear and death by diffusion, *Deep Sea Res., Part I*, *55*, 277–295.

Cowles, T. J. (2003), Planktonic layers: Physical and biological interactions on the small scale, in *Handbook of Scaling Methods in Aquatic Ecology: Measurements, Analysis, Simulation*, edited by L. Seuront and P. G. Strutton, pp. 31–49, CRC Press, Boca Raton, Fla.

Cowles, T. J., and R. A. Desiderio (1993), Resolution of biological microstructure through in situ fluorescence emission spectra: An oceanographic application using optical fibers, *Oceanography*, *6*, 105–111.

Cowles, T. J., R. A. Desiderio, and M. E. Carr (1998), Small-scale planktonic stucture: Persistence and trophic consequences, *Oceanography*, *11*(1), 4–9.

Davis, R. E., C. E. Eriksen, and C. P. Jones (2002), Autonomous buoyancy-driven underwater gliders, in *The Technology and Applications of Autonomous Underwater Vehicles*, edited by G. Griffiths, pp. 37–58, Taylor and Francis, London, U. K.

Dekshenieks, M. M., P. L. Donaghay, J. M. Sullivan, J. E. B. Rines, T. R. Osborn, and M. S. Twardowski (2001), Temporal and spatial occurrence of thin phytoplankton layers in relation to physical processes, *Mar. Ecol. Prog. Ser.*, *223*, 61–71.

Derenbach, J. B., H. Astheimer, H. P. Hansen, and H. Leach (1979), Vertical microscale distribution of phytoplankton in relation to the thermocline, *Mar. Ecol. Prog. Ser.*, *1*, 187–193.

Donaghay, P. L., H. M. Rines, and J. M. Sieburth (1992), Simultaneous sampling of fine scale biological, chemical, and physical structure in stratified waters, *Arch. Hydrobiol.*, *36*, 97–108.

Eckart, C. (1948), An analysis of the stirring and mixing processes in incompressible fluids, *J. Mar. Res.*, *7*, 265–275.

Falkowski, P. G., and Z. Kolber (1995), Variations in chlorophyll fluorescence yields in phytoplankton in the world oceans, *Aust. J. Plant Physiol.*, *22*(2), 341–355.

Fiorelli, E., N. E. Leonard, P. Bhatta, D. Paley, R. Bachmayer, and D. M. Fratantoni (2004), Multi-AUV control and adaptive sampling in Monterey Bay, in *Proc. IEEE Autonomous Underwater Vehicles 2004: Workshop on Multiple AUV Operations*, pp. 134–147, IEEE, Piscataway, NJ.

Franks, P. J. S. (1995), Thin layers of phytoplankton: A model of formation by near-inertial wave shear, *Deep Sea Res., Part I*, *42*(1), 75–83.

Fratantoni, D. M., and R. E. Davis (2003), Autonomous underwater glider performance during AOSN-II, *Eos Trans. AGU*, *84*(52), Ocean Sci. Meet. Suppl., Abstract OS22D-01.

Gargett, A. E., P. J. Hendricks, T. B. Sanford, T. R. Osborn, and A. J. Williams (1981), A composite spectrum of vertical shear in the upper ocean, *J. Phys. Oceanogr.*, *11*(9), 1258–1271.

Hoerner, S. F. (1965), *Fluid Dynamic Drag*, Horner Books, Midland Park, N. J.

Krause, G. H., and E. Weis (1991), Chlorophyll fluorescence and photsythesis: The basics, *Annu. Rev. Plant Physiol. Plant Mol. Biol.*, *42*, 313–349.

McManus, M. A., et al. (2003), Characteristics, distribution and persistence of thin layers of a 48 hour period, *Mar. Ecol. Prog. Ser.*, *261*, 1–19.

Osborn, T. R. (1988), Signatures of doubly diffusive convection and turbulence in an intrusive regime, *J. Phys. Oceanogr.*, *18*(1), 145–155.

Rudnick, D. L., R. E. Davis, C. C. Eriksen, D. M. Fratantoni, and M. J. Perry (2004), Underwater gliders for ocean research, *Mar. Technol. Soc. J.*, *38*(1), 48–59.

Strickland, J. D. H. (1968), A comparison of profiles of nutrient and chlorophyll concentrations taken from discrete depths and by continuous recording, *Limnol. Oceanogr.*, *13*(2), 388–391.

Zaneveld, J. R. V., and W. S. Pegau (1998), A model for the reflectance of thin layers, fronts, and internal waves and its inversion, *Oceanography*, *11*(1), 44–47.

D. M. Fratantoni and B. A. Hodges, Autonomous Systems Laboratory, Department of Physical Oceanography, Woods Hole Oceanographic Institution, Woods Hole, MA 02543, USA. (bhodges@whoi.edu)